Biosensors and Bioelectronics 146 (2019) 111768

Contents lists available at ScienceDirect

Biosensors and Bioelectronics

journal homepage: http://www.elsevier.com/locate/bios

An ultrasensitive ratiometric electrochemiluminescence immunosensor combining photothermal amplification for ovarian cancer marker detection

Dandan Fang [a,1], Shupei Zhang [b,1], Hong Dai [a,b,*], Yanyu Lin [a]

[a] College of Chemistry and Material, Fujian Normal University, Fuzhou, Fujian, 350108, China
[b] Fujian Provincial Maternity and Children's Hospital, Affiliated hospital of Fujian Medical University, Fuzhou, Fujian, 350108, China

ARTICLE INFO

Keywords:
ECL immunosensor
HE4
Photothermal effect
Semiconducting polymer dots
CNHs

ABSTRACT

Signal amplification strategies play important functions in the development of highly sensitive electrochemiluminescence (ECL) immunosensing system. Herein, a photothermal enhanced ratiometric ECL immunosensor was proposed for the detection of human epididymis protein 4 (HE4), an ovarian cancer biomarker. Mesoporous SiO_2 (ms-SiO_2) and carbon nanohorns (CNHs) was served as carrier of ECL emitter carbon nitride nanosheet (g-C_3N_4) and anodic ECL emitter polymer dots (Pdots), respectively. The large specific area of ms-SiO_2 and CNHs improved the loading capacity of g-C_3N_4 and Pdots, enhancing ECL signals. Furthermore, CNHs was innovatively utilized as thermal convert unit to increase the electrode surface temperature, which benefited from its extraordinary photothermal property at 808 nm that can convert laser energy into heat for elevating the temperature, further amplified ECL signal. The delicately designed ECL immunosensor exhibited excellent sensitivity to HE4 detection with wide linear range from 1.0×10^{-5} to 10 ng/mL and low detection limit of 3.3×10^{-6} ng/mL. This work not only provided an effective way to develop highly sensitive ECL immunosensor but could attract more attention on the application of photothermal material in the ECL field.

1. Introduction

Ovarian cancer is one of the most lethal cancers among all gynecological malignancies, seriously threatening the human health (Tajmul et al., 2018; Zuo et al., 2018a,b). Due to the lack of specific symptoms, most ovarian cancer patients were diagnosed at an advanced stages of III and IV, the 5-year survival rate was low to 40% (Franier and Thompson, 2019; Lu, 2018). Therefore, finding an effective biomarker has a vital significance for ovarian cancer early diagnosis to improve the survival of patients. Studies showed that human epididymis protein 4 (HE4) is an important biomarker of ovarian cancer (Granato et al., 2015). Currently, a variety of analytical techniques such as electrochemical immunosensor (Fan et al., 2019), chemiluminescence immunoassay (Fu et al., 2018), photoelectrochemical sensing (Tan et al., 2018) have been proposed for the determination of HE4. Electrochemiluminescence (ECL), a promising technique combining the advantages of both electrochemical and chemiluminescent, has been widely employed for biomarkers analysis because of its high sensitivity, rapidness, easy controllability and low background signal (Hu et al., 2019). Although possessing attractive merits of this method, single-signal ECL measurement might cause some false positive or negative errors due to instrumental efficiency or environmental change (Tan et al., 2018).

Accordingly, much effort was committed to the construction of ratiometric ECL immunosensor for bioanalysis, which can efficiently eliminate interferences from variable external environment by self-calibration of two ECL signals, making the detection results more convincing (Zuo et al., 2018a,b). Finding a pair of potential-resolved emitters is especially important to develop ratiometric immunosensor. Semiconducting polymer dots were a new kind of luminophore, which possessed high luminescence efficiency, excellent photostability and photothermal performance (Sheydaei et al., 2018; Sun et al., 2017), showing an attractive application in biological imaging, biosensing and photothermal therapy. However, polymer dots had disadvantage of poor water solubility (Li et al., 2018). Therefore, a tetraphenylporphyrin (TPP)-doped conjugated polymer poly [(9,9-dioctylfluorenyl-2, 7-diyl)-co-(1,4-benzo-{2,1′,3}-thiadazole)] (PFBT) polymer dots (abbreviated as Pdots) with abundant carboxyl group, favorable water solubility and good biocompatibility were prepared in this work, which can produce strong anodic ECL signal in the presence of tripropylamine (TPrA). Carbon nitride nanosheet (g-C_3N_4), a kind of metal-free

* Corresponding author. College of Chemistry and Material, Fujian Normal University, Fuzhou, Fujian, 350108, China.
E-mail address: dhong@fjnu.edu.cn (H. Dai).
[1] The author contributed to the work equally and should be regarded as co-first author.

https://doi.org/10.1016/j.bios.2019.111768
Received 23 July 2019; Received in revised form 26 September 2019; Accepted 7 October 2019
Available online 8 October 2019

semiconductor nanoparticles with excellent catalytic, optical and electronic properties, was chosen as cathodic luminophore in this work (Hu et al., 2018; Sha et al., 2019). However, there was currently no report based on Pdots and g-C_3N_4 ECL pair for bioassay.

It is well known that enhancing the ECL signal could improve the sensitivity of the biosensor (Gai et al., 2018). The most common method to boost biosensor sensitivity is to introduce coreactant into ECL system or increase the loading amount of luminophore (Chen et al., 2018; Zhang et al., 2019). Additionally, studies showed that the increase of electrode surface temperature could enhance ECL signal and improve sensitivity of the immunosensor (Zhang et al., 2018). Therefore, the development of an effective method to elevate the electrode surface temperature is urgently desirable. Herein, the photothermal material was innovatively utilized as thermal convertor device, which can effectively convert 808 nm laser energy into heat, resulting in an increase of the electrode surface temperature, and then promoted the performance of the sensor by affecting thermodynamic and kinetic parameters of the reaction (Zhang et al., 2019). Carbon-based nanomaterials with strong near-infrared (NIR) harvesting capability were a class of excellent photothermal reagent (Fu et al., 2016). Among various carbon-based nanomaterials, carbon nanohorns (CNHs) received substantial attention due to its distinctive conical morphology, good biocompatibility, large specific surface area, and extraordinary photothermal property (Dai et al., 2013). Moreover, compared with other carbon nanomaterials, CNHs owned high aspect ratio and favorable micropores (Wang et al., 2019). Thus CNHs was used as a prominent nanocarrier, which could improve the immobilized quantity of luminophore and accelerate electron transfer, as well as increase the electrode surface temperature.

In this work, a photothermal enhanced ratiometric ECL immunosensor was constructed for HE4 determination by employing g-C_3N_4@ms-SiO_2 as the sensing platform and Pdots@CNHs as photothermal probe. G-C_3N_4@ms-SiO_2 as cathodic ECL emitter was modified onto the electrode, providing substantial immobilization sites for antibodies (Ab_1). Pdots@CNHs as anodic ECL emitter could effectively convert laser energy into heat to elevate electrode surface temperature, amplifying ECL signal and improving sensitivity of the immunosensor. Therefore, a highly-efficient ratiometric ECL immunosensor based on photothermal amplification was proposed, which exhibited high sensitivity and good selectivity for HE4 analysis. More importantly, this work provided a promising method for the detection of other biomarkers in clinical diagnosis.

2. Experimental

2.1. Materials

Poly (styrene-co-maleic anhydride) (PSMA) was purchased from Heowns Biochem LLC (Tianjin, China). The conjugated polymer poly [(9,9-dioctylfluorenyl −2,7-diyl)-co-(1,4-benzo-thiadazole)] (PFBT) and the photosensitizer tetraphenylporphyrin (TPP) were obtained from Sigma-Aldrich Co., Ltd (USA). N-Hydroxy succinimide (NHS, GR) and 1-ethyl-3-(3-di-methylaminopropyl) carbodiimide hydrochloride (EDC, GR) were acquired from Shanghai Medpep Co., Ltd (Shanghai, China). Bovine serum albumin (BSA, 96–99%, GR) was purchased from Biss Inc. (Beijing, China). Antigen and antibody of human epididymis protein 4 (HE4) were offered by San Ying Biotechnology Co., Ltd (Wuhan, China). A-fetoprotein (AFP), carcinoembryonic antigen (CEA) and carbohydrate antigen 199 (CA199) were supplied by Linc-Bio Science Co., Ltd (Shanghai, China). The human serum sample was provided by Fujian Provincial Maternity and Children's Hospital. The phosphate buffer solution (PBS, 0.1 M) with different pH were prepared by mixing stock solution of 0.1 M NaH_2PO_4 and 0.1 M Na_2HPO_4 and adjusted the pH.

2.2. Apparatus

Cyclic voltammetry and electrochemical impedance spectroscopy (EIS) experiments were conducted on CHI760 electrochemical workstation (Shanghai Chenhua Instrument Co., Shanghai, China). The ECL emission measurements were performed on a model MPI-E ECL analyzer (Xi'an Remax Analysis Instrument Co., Xi'an, China) in conjunction with a CHI600E electrochemical workstation (Shanghai Chenhua Instrument Co., Shanghai, China). The experiments applied a conventional three-electrode system with a modified glass carbon electrode (GCE, $d = 3$ mm) as the working electrode, a platinum wire as auxiliary electrode ($d = 1$ mm) and an Ag/AgCl as the reference electrode. The electrode temperature was regulated by an 808 nm NIR light system at a laser power density of 2.0 W/cm^2, the temperature was monitored using a pen-style digital thermometer. Scanning electron microscopy (SEM, SU8000 instrument) and transmission electron microscopy (TEM, FEI F20 S-TWIN instrument) were employed to characterize the morphology of the materials.

2.3. Synthesis of TPP-doped PFBT Pdots

The TPP-doped PFBT Pdots were prepared as previously reported (Li et al., 2017). The PFBT polymer (1 mg/mL), functional polymer PSMA (1 mg/mL), and photosensitizer TPP (1 mg/mL) were dissolved into THF to obtain the mixed solution (100 μg/mL PFBT, 20 μg/mL PSMA, 5 μg/mL TPP). And then the mixed solution was ultrasonically treated to form a homogenous solution. Subsequently, 2 mL mixed solution was quickly added into the 10 mL ultrapure water under ultrasonic. Afterwards, THF was removed by nitrogen stripping and the obtained solution was filtered through a 0.22 μm filter. Ultimately, the final product was acquired by rotary evaporation under 55 °C.

2.4. Preparation of g-C_3N_4@ms-SiO_2 composites

The g-C_3N_4 was synthesized according to previous report with some modification (Lin et al., 2018; Melchior et al., 2019). 5 g melamine was added into an alumina crucible with a lid and heated at 600 °C for 4 h with a heating rate of 5 °C/min to obtain the yellow powder. Afterwards, 1 g of g-C_3N_4 was added into the mixed acid (VH_2SO_4:$VHNO_3$ = 3:1), and continuously stirred for 12 h. After washed with ultrapure water until pH reached 7.0, the solution was dried at 35 °C for 12 h and acquired the carboxyl wrapped g-C_3N_4. The preparation process of mesoporous SiO_2 (ms-SiO_2) was displayed in the Supporting Information. 100 μL of prepared g-C_3N_4 (3 mg/mL) was added into 100 μL of ms-SiO_2 (3 mg/mL) and stirred for 5 h. After that, the g-C_3N_4@ms-SiO_2 composites was obtained via centrifugation and washed with ultrapure water.

2.5. Preparation of Ab_2 bioconjugates

Initially, 5 mg CNHs was dissolved into 1 mL N,N-Dimethylformamide (DMF) with ultrasonic treatment for 30 min. Subsequently, 200 μL of 5 mg/mL CNHs was mixed with 200 μL of 5 mg/mL carboxyl-capped Pdots and kept stirring for 5 h to enable enough Pdots adsorbed on CNHs. After washed with ultrapure water to remove excess Pdots, 100 μL mixed solution of EDC/NHS (40 mM/10 mM) was used to activate the carboxyl group in Pdots@CNHs for 1 h. Followed by adding 100 μL of 50 μg/mL Ab_2 and stirring for 50 min. The Pdots@CNHs-Ab_2 bioconjugates was formed based on the amine reaction between the carboxyl on Pdots@CNHs and the amino on Ab_2, which was collected via centrifugation and washed with ultrapure water. Finally, 50 μL of 1 wt% BSA was added into Pdots@CNHs-Ab_2 bioconjugates to block the remaining active sites. After centrifugal washing, the Pdots@CNHs-Ab_2-BSA (Ab_2 bioconjugates) was prepared and stored at 4 °C for further use.

2.6. Fabrication procedure of ratiometric ECL biosensor

The fabrication process of the ratiometric ECL immunosensor was shown in Scheme 1. Prior to modification, the GCE was polished according to previous method (Fu et al., 2019). Then 3 μL of 3 mg/mL g-C_3N_4@ms-SiO_2 was dropped onto the cleaned GCE and dried at room temperature. Subsequently, 10 μL of EDC/NHS (40 mM/10 mM) solution was used to activate the carboxyl group of g-C_3N_4@ms-SiO_2 for 40 min. After washed with ultrapure water, 3 μL of 50 μg/mL antibody (Ab_1) was incubated on the modified electrode for 40 min at room temperature. And then removed excess reagent, 3 μL of 1.0 wt% BSA was dipped onto the modified electrode to block the nonspecific adsorption sites. Subsequently, 3 μL of HE4 with different concentrations was added on the decorated electrode and incubated for 30 min at room temperature. After washed with ultrapure water, 3 μL Ab_2 bioconjugates was incubated on the modified electrode for 50 min at room temperature to construct ratiometric ECL immunosensor. The layout of the laser regulated temperature was shown in Scheme S1.

3. Results and discussion

3.1. Characterizations of materials

To investigate the morphology and structure of Pdots, the TEM image was provided. From Fig. 1A, quasi-spherical particles with the diameter of ~3 nm and uniform morphology were observed, which was favorable for the formation of uniform photoresponsive film and steady signals. Besides, the UV–Vis absorption spectrum of Pdots was displayed in Fig. 1B (blue curve), the Pdots had two obvious adsorption peaks at 323 nm and 460 nm. And the red curve in Fig. 1B depicted the fluorescence spectra of Pdots, the emissions at 675 nm and the shoulder peak at 725 nm were attributed to the characteristic emission of the TPP dopant, the small emission peak at 550 nm was assigned to the emission of pure PFBT polymer, which was quenched dramatically in the presence of TPP dopant due to the combined effects of energy diffusion and energy transfer (Li et al., 2017; Shi et al., 2018). Furthermore, the inset in Fig. 1B showed the digital and fluorescence images of Pdots, the color of the Pdots dispersion solution changed from yellow to orange-red after the excitation of a 365 nm UV lamp. All above results indicated the successful preparation of the Pdots.

The morphology of ms-SiO_2 was characterized by SEM and TEM. It can be seen clearly in SEM image (Fig. S1A) that the surface of ms-SiO_2 was comparatively rough, which could provide substantial immobilization sites for molecules. The TEM image of ms-SiO_2 was displayed in Fig. S1B, the ms-SiO_2 was spherical shape with the average particle size of 68 nm and its surface possessed numerous irregular craters. In addition, the SEM image of g-C_3N_4 was exhibited in Figs. S1C and a large number of smooth nanosheets stacked together, which endowed g-C_3N_4 large specific surface area.

3.2. Feasibility of the constructed immunosensor

To demonstrate two luminophores had no interplay in the potential range of −1.3–1.3 V, a series of experiments were carried out as illustrated in Fig. 2A. There was only one ECL signal was obtained (−1.3 V, curve a) when g-C_3N_4@ms-SiO_2, $S_2O_8^{2-}$ and TPrA were added into PBS (pH 8.0). Moreover, Fig. S2B has demonstrated the enhancement in ECL signal of g-C_3N_4@ms-SiO_2 was caused by $S_2O_8^{2-}$ not TPrA. Therefore, the ECL signal at −1.3 V was the result of the reaction of g-C_3N_4@ms-SiO_2 and $S_2O_8^{2-}$. When Pdots@CNHs, $S_2O_8^{2-}$ and TPrA all existed in PBS (pH 8.0), only one ECL signal appeared (1.2 V, curve b). Fig. S2A has proved that the enhancement of Pdots@CNHs signal was attributed to TPrA. Hence, the ECL signal at 1.2 V was the result of the reaction of Pdots@CNHs and TPrA. Two ECL signals were obtained when the luminophores (g-C_3N_4@ms-SiO_2 and Pdots@CNHs) and the coreactants ($S_2O_8^{2-}$ and TPrA) were simultaneously added into PBS (pH 8.0), and which had no significant change in comparison with that of curve a and curve b. Aforementioned phenomena indicated that the dual ECL signal system possessed two independent ECL signal even though the detection solution existed two kinds of coreactants.

The ECL responses of different modified electrodes were investigated in 0.1 M PBS (pH 8.0) containing 15 mM TPrA and 10 mM $S_2O_8^{2-}$. As shown in Fig. 2B, g-C_3N_4@ms-SiO_2 modified electrode showed an ECL signal of 11025 a.u. (curve a). However, the ECL signal decreased to 7992 a.u. (curve b) after modification of Ab_1 on the above electrode. After target HE4 was incubated onto the electrode, the ECL intensity further reduced to 6047 a.u. (curve c). Interestingly, when Ab_2 bioconjugates was attached to the electrode, a new ECL signal of 4652 a.u. appeared (curve d), which was attributed to the ECL emission of Pdots@CNHs, however, the ECL signal of g-C_3N_4@ms-SiO_2 decreased sharply to 3389 a.u. Delightedly, the ECL intensity of Pdots@CNHs and g-C_3N_4@ms-SiO_2 both enhanced significantly (curve e) when the sensor was irradiated by 808 nm laser for 30 s. Above results demonstrated the successful construction of the ECL immunosensor, and exhibited an effective method for amplifying ECL signal.

EIS as a powerful technique was used to investigate the fabrication process of this immunosensor. In the EIS Nyquist plots, the semicircle diameter represents the electron-transfer resistance (R_{et}). As presented

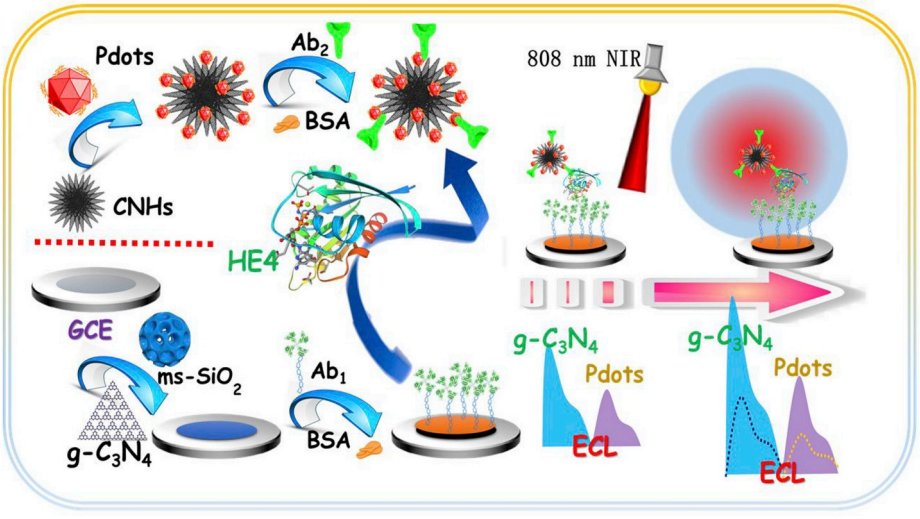

Scheme 1. The schematic illustration of the ECL immunosensor.

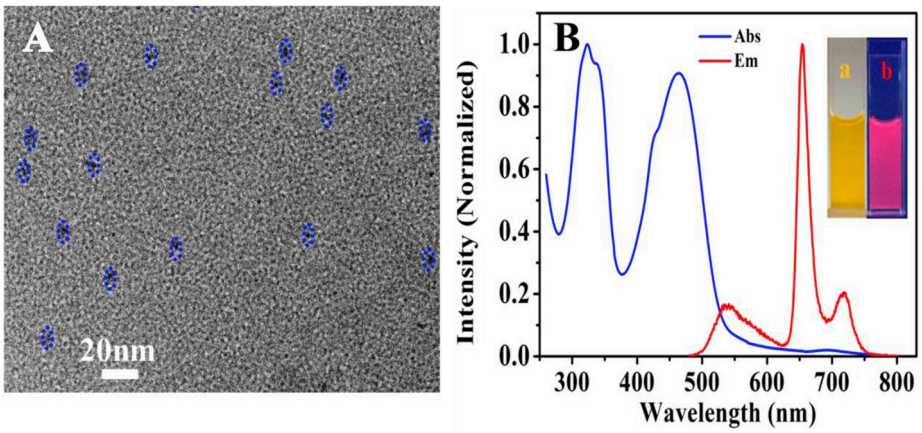

Fig. 1. (A) TEM image of Pdots. (B) Normalized absorption and emission spectra of the Pdots. Inset in B was the image of Pdots under white light and UV light irradiation (λex = 365 nm).

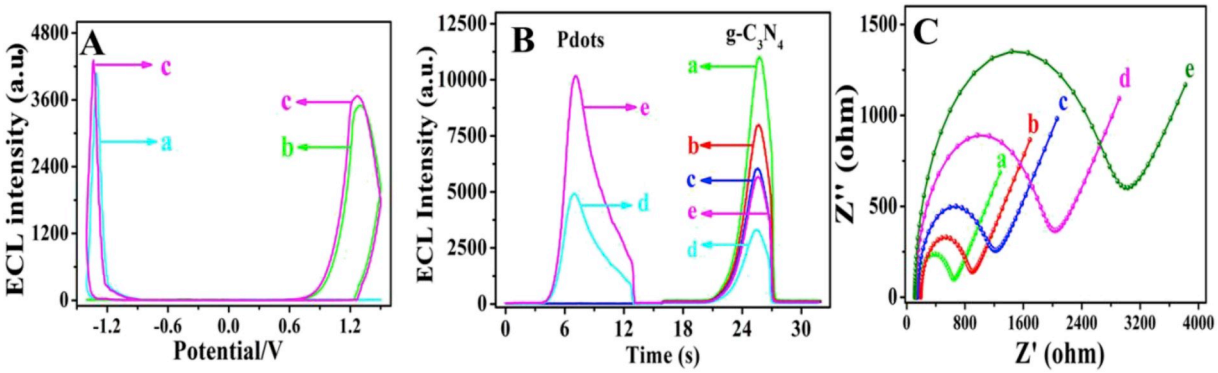

Fig. 2. (A) ECL-potential curves of bare GCE in 0.1 M PBS (pH 8.0) containing different components. (B) ECL responses of different modified electrodes: (a) g-C_3N_4@ms-SiO_2/GCE, (b) Ab_1/g-C_3N_4@ms-SiO_2/GCE, (c) HE4/BSA/Ab_1/g-C_3N_4@ms-SiO_2/GCE, (d) Ab_2 bioconjugates/HE4/BSA/Ab_1/g-C_3N_4@ms-SiO_2/GCE, and (e) irradiated Ab_2 bioconjugates/HE4/BSA/Ab_1/g-C_3N_4@ms-SiO_2/GCE by an 808 nm laser at a power density of 2.0 W/cm^2 for 30 s. All the measurements were performed in 0.1 M PBS (pH 8.0) containing 15 mM TPrA and 10 mM $S_2O_8^{2-}$. (C) EIS profiles of (a) GCE, (b) g-C_3N_4@ms-SiO_2/GCE, (c) Ab_1/g-C_3N_4@ms-SiO_2/GCE, (d) HE4/BSA/Ab_1/g-C_3N_4@ms-SiO_2/GCE, (e) Ab_2 bioconjugates/HE4/BSA/Ab_1/g-C_3N_4@ms-SiO_2/GCE in 0.1 M KCl containing 5.0 mM $[Fe(CN)_6]^{3-/4-}$.

in Fig. 2C, the bare GCE had a small R_{et} value of 645 Ω (curve a). While the R_{et} value increased to 897 Ω (curve b) when g-C_3N_4@ms-SiO_2 was modified on the electrode, owing to the poor conductivity of g-C_3N_4 and ms-SiO_2 impeded the electron transfer. After successive incubation of Ab_1, HE4 and Ab_2 bioconjugates, due to the insulation effect of protein molecule which obstructed the electron transport, the R_{et} increased to 1211 Ω (curve c), 2031 Ω (curve d) and 3033 Ω (curve e), respectively. The changes of R_{et} values confirmed the successful construction of ECL immunosensor.

3.3. The ECL behavior regulated by temperature

To give insight of the effect of the laser irradiation on the ECL responses of Pdots@CNHs and g-C_3N_4@ms-SiO_2, a series of related experiments were conducted. As exhibited in Fig. 3A, the ECL intensity of Pdots@CNHs and g-C_3N_4@ms-SiO_2 was 2.5 times and 1.5 times higher than those without laser irradiation, respectively. The signal enhancement in Pdots@CNHs and g-C_3N_4@ms-SiO_2 might relate with the increase of electrode surface temperature. As a proof of our conjecture, the ECL responses of Pdots@CNHs and g-C_3N_4@ms-SiO_2 were recorded under continuous irradiation as shown in Fig. 3B. The ECL signals of Pdots@CNHs and g-C_3N_4@ms-SiO_2 both enhanced gradually with the prolongation of irradiation time, which certified that elevating temperature could enhance the ECL responses. To further explore the influence of temperature, Fig. 3C showed the electrochemical behaviors of CNHs@Pdots modified electrodes at different temperatures. $[Fe(CN)_6]^{3-/4-}$ was used as redox probe, the redox peaks current increased with an increase of the electrode surface temperature, the reason might be that the increase of electrode surface temperature caused a decrease in viscosity around the electrode surface, and then accelerated the diffusion and improved the redox current of electroactive species (Lichan et al., 2009). Furthermore, the peak current increased linearly with the square root of the scan rate in the range of 0.09–1.0 V/s (Fig. 3D), indicating the redox of $[Fe(CN)_6]^{3-/4-}$ on CNHs@Pdots modified electrode was a typical diffusion controlled process. The slope and the standard heterogeneous rate constant (k_s) of regression curve at 40 °C was larger than that at 35 °C and 30 °C (the ratio of k_s was about 3.4 (40 °C): 2.7 (35 °C): 1.7 (30 °C)), indicating the increase of the electrode surface temperature can promote electrochemical reaction.

3.4. Investigation of photothermal device and the effect on the ECL system

Though fore-mentioned experiments have proved that increasing the electrode surface temperature can amplify ECL signal, the main contributor for temperature did not point out definitely. Thus, the photothermal performances of different materials were investigated with ultrapure water as control sample in Fig. 4A. The temperature of g-C_3N_4 solution and ms-SiO_2 solution had no obvious changes in comparison with ultrapure water, while the temperature of Pdots solution and CNHs solution increased up to 41.3 °C and 78.3 °C upon laser irradiation for 10 min. More impressively, the temperature of CNHs@Pdots increased up to 91.4 °C, indicating excellent photothermal effect of

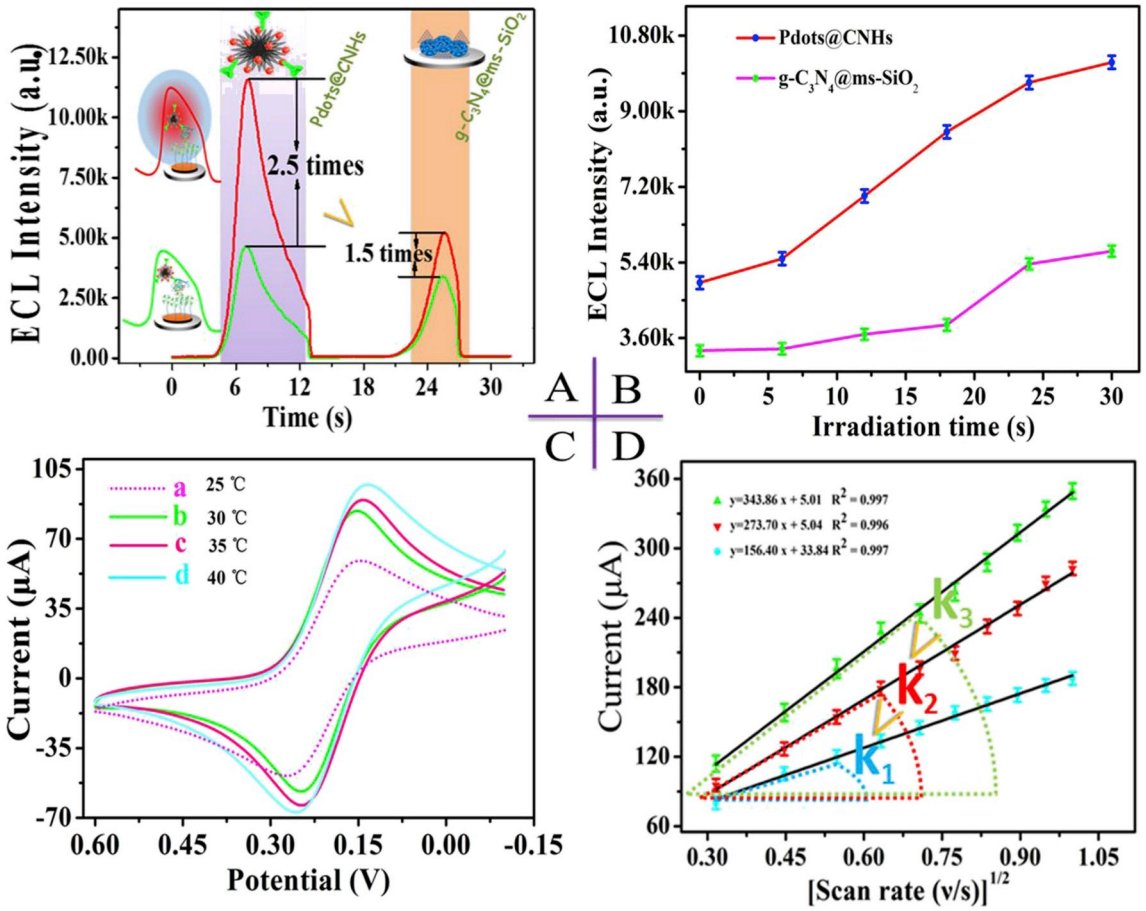

Fig. 3. (A) The ECL signals of Pdots@CNHs and g-C_3N_4@ms-SiO_2 before and after 808 nm laser irradiation. (B) The variation of the ECL intensities of Pdots@CNHs and g-C_3N_4@ms-SiO_2 under 808 nm laser irradiation. (C) The cyclic voltammograms of Pdots@CNHs/GCE in 0.1 M KCl containing 5.0 mM $[Fe(CN)_6]^{3-/4-}$ at different temperatures. (D) The linear relationship between the peak currents and the square root of scan rate at different temperatures.

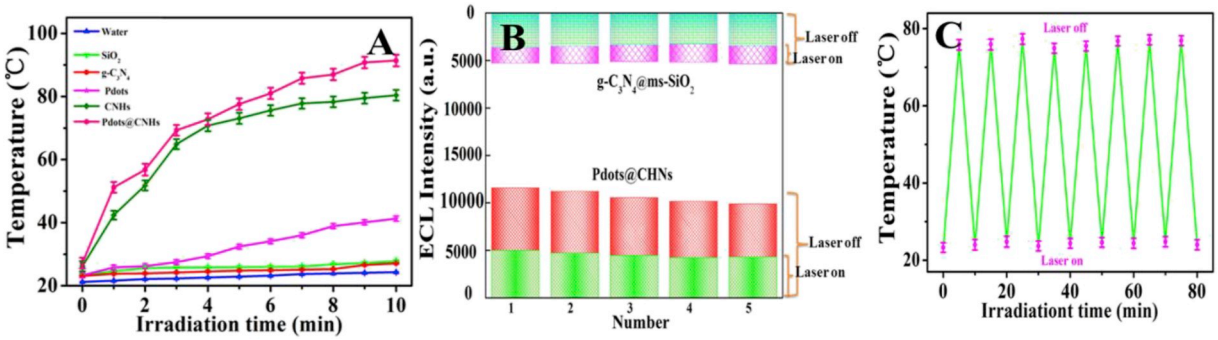

Fig. 4. (A) Temperature comparison of different materials under an 808 nm laser irradiation over a period of 10 min. (B) The change of Pdots@CNHs and Pdots@CNHs ECL signal over 5 irradiation cycles. (C) The photostability of Pdots@CNHs.

CNHs@Pdots. Taking into consideration the bioactivity, the laser irradiation time was set at 30 s (the temperature was about 37 °C).

In addition, as illustrated in Fig. 4B, the ECL signal of the g-C_3N_4@ms-SiO_2 and Pdots@CNHs both enhanced significantly with laser irradiation. Moreover, the extent of increase (Laser off-laser on) of Pdots@CNHs signal was higher than that of g-C_3N_4@ms-SiO_2, which was consistent with the results in Figs. 2B and 3A. The reasons might be that the Pdots@CNHs possessed excellent photothermal property, which can act as thermal convert device to increase the electrode surface temperature by converting laser energy into heat, and then a temperature gradient layer was formed near the electrode surface at high electrode surface temperature, which would improve the diffusion and convection of the active compounds to electrode surface, resulting in the amplification in ECL signal (Lin et al., 2010). However, the g-C_3N_4@ms-SiO_2 was served as the sensing platform, which did not directly contact with thermal convert unit Pdots@CNHs. The signal amplification in g-C_3N_4@ms-SiO_2 mainly caused by the thermal radiation from Pdots@CNHs, therefore the increase range of ECL signal of g-C_3N_4@ms-SiO_2 was lower than that of Pdots@CNHs. Satisfyingly, the ECL intensity of g-C_3N_4@ms-SiO_2 and Pdots@CNHs kept a relatively stable value upon 5 continuous laser on/off cycles. Besides, the photostability of Pdots@CNHs composites was investigated upon 9 continuous laser on/off cycles in Fig. 4C, there was no obvious distinction of maximum temperature elevation, indicating a good photostability of

Pdots@CNHs composites.

3.5. Optimization the experimental conditions

In order to achieve high sensitivity of HE4 detection, several conditions were optimized at room temperature, including the concentration of $S_2O_8^{2-}$ and TPrA, the immobilization time of g-C_3N_4 on ms-SiO_2 and Pdots on CNHs, the incubation time of Ab_1, HE4, and Ab_2 bioconjugates, as well as the pH of detection solution. The corresponding results were exhibited in the Supporting Information. 10 mM and 15 mM were chosen as the optimal concentration of $S_2O_8^{2-}$ and TPrA, respectively. The optimal immobilization time of g-C_3N_4 on ms-SiO_2 and Pdots on CNHs were both 5 h 40 min, 30 mim and 50 min was selected as the optimal incubation time of Ab_1, HE4 and Ab_2 bioconjugates, respectively. pH 8.0 was chosen as the optimal pH.

3.6. Analytical performance of the developed ratiometric biosensor

Under optimal conditions, different concentrations of HE4 were detected by the constructed immunosensor as illustrated in Fig. 5A. The cathodic ECL intensity declined while the anodic ECL intensity increased with the augment of the concentration of HE4 from 1.0×10^{-5} ng/mL to 10 ng/mL. The ratio of anodic to cathodic (Ia/Ic) and the logarithm of HE4 concentrations exhibited an excellent linear relationship (Fig. 5B). The linear equation was I = 2.183 + 0.369 logC ($R^2 = 0.995$) with a detection limit of 3.3×10^{-6} ng/mL (S/N = 3). Compared with other detection methods (Table S1), the proposed immunosensor showed a wider linear range and a lower detection limit for HE4 detection, demonstrating that the proposed immunosensor can be used to sensitively detect HE4.

Selectivity was an important criterion for evaluating the analytical performance of the ECL immunosensor. AFP, CEA, and CA 199 are common interfering biomolecules in serum, which exist in the blood of both patient and normal human. Therefore, the ECL responses of potential interferences were researched. As shown in Fig. 5C, the ECL responses of the interferences were very weak and nearly identical to the blank sample. While a high ECL response was obtained in the presence of HE4. Moreover, the ECL response of mixture containing three interferences and HE4 had no prominent disparity compared to HE4 only. Above results illustrated that the constructed ratiometric ECL immunosensor possessed an excellent selectivity.

The reproducibility of this immunosensor was investigated by detecting HE4 (1 ng/mL) using six electrodes prepared under the same conditions. As exhibited in Fig. 5D, the relative standard detection (RSD) was 3.69%, indicating an acceptable reproducibility of the constructed immunosensor.

3.7. Analysis of HE4 in human serum sample

The practical application of the developed immunosensor was evaluated in human serum samples by using standard addition method. Human serum samples were diluted by 0.1 M PBS (pH 7.4) before the detection. Subsequently, HE4 with different concentrations was added into diluted human serum samples and then detected by the constructed immunosensor. The results were listed in Table S2, the recoveries were ranged from 102.1% to 107.8%, implying that the designed ECL immunosensor had a great potential application for HE4 detection in clinical analysis.

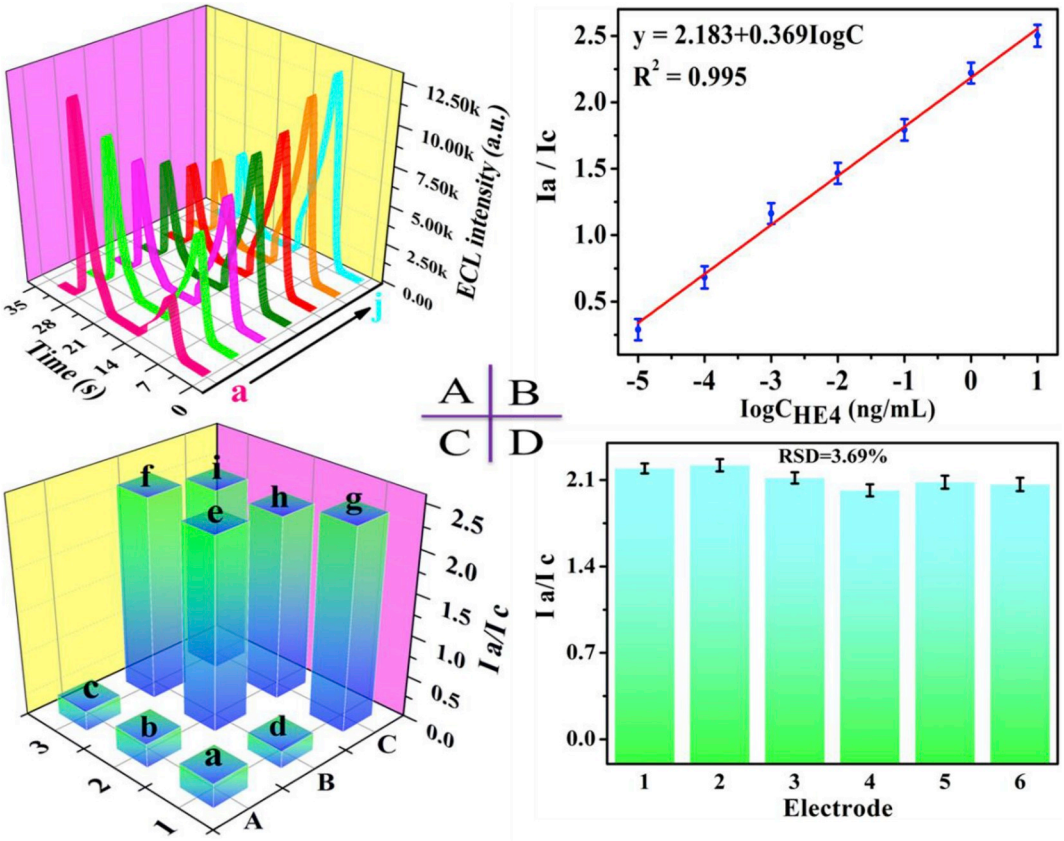

Fig. 5. (A) The ECL signals of the immunosensor with different concentrations of HE4 (a–j: 10^{-5}-10 ng/mL) in 0.1 M PBS (pH 8.0) containing 15 mM TPrA and 10 mM $S_2O_8^{2-}$. (The laser irradiation was 30 s) (B) The corresponding calibration curve for HE4 detection. (C) Selectivity of the proposed immunosensor toward different interferences: (a) blank, (b) AFP, (c) CEA, (d) CA199, (e) HE4, (f) HE4+AFP, (g) HE4 +CEA, (h) HE4 +CA199, (i) mixture. (D) The reproducibility tests of six modified electrodes incubated with 1 ng/mL HE4.

4. Conclusion

In summary, an ultrasensitive ratiometric ECL immunosensor combining with photothermal amplification was developed. The constructed immunosensor showed excellent performance such as high sensitivity, low detection limit and wide linear range for HE4 determination. Highlights of the immunosensor can be simply summarized as follows: (1) A novel ECL pair, CNHs@Pdots and g-C_3N_4@ms-SiO_2, was introduced to ratiometric ECL bioanalysis for the first time. (2) The large surface area of CNHs and ms-SiO_2 increased the immobilization amount of Pdots and g-C_3N_4, resulting in the enhancement of ECL signal. (3) CNHs possessed extraordinary photothermal property, which was used as thermal convert device to increase the electrode surface temperature, amplifying ECL signal and improving detection sensitivity. However, the utilization of cut-off filter for improving the noise-signal ratio in this work might weaken the ECL signal to some extent, which encouraged us to explore an effective method to decrease the adverse effect of cut-off filter on ECL signal.

Declaration of competing interest

The authors declare that they have no known competing financial interests or personal relationships that could have appeared to influence the work reported in this paper.

CRediT authorship contribution statement

Dandan Fang: Investigation. **Shupei Zhang:** Writing - original draft. **Hong Dai:** Funding acquisition, Methodology, Project administration. **Yanyu Lin:** Data curation, Formal analysis.

Acknowledgment

This project was financially supported by the NSFC (21877012, 21575024), National Science Foundation of Fujian Province (2016J06003, 2016J05026, 2017J01620, 2016J01429) and Education Department of Fujian Province (JK2016009, FBJG20170186, JA14071) was also greatly acknowledged.

Appendix A. Supplementary data

Supplementary data to this article can be found online at https://doi.org/10.1016/j.bios.2019.111768.

References

Chen, Z., Han, Y., Li, T., Zhang, X., Wang, T., Zhang, Z., 2018. Mater. Lett. 220, 305–308.
Dai, H., Gong, L., Xu, G., Zhang, S., Lu, S., Jiang, Y., Lin, Y., Guo, L., Chen, G., 2013. Electrochim. Acta 111, 57–63.
Fan, L., Yan, Y., Guo, B., Zhao, M., Li, J., Bian, X., Wu, H., Cheng, W., Ding, S., 2019. Sens. Actuators B Chem. 296, 126697.
Franier, B.D.L., Thompson, M., 2019. Biosens. Bioelectron. 135, 71–81.
Fu, G., Sanjay, S.T., Dou, M., Li, X., 2016. Nanoscale 8, 5422–5427.
Fu, X., Liu, Y., Qiu, R., Foda, M.F., Zhang, Y., Wang, T., Li, J., 2018. Biochem. Biophys. Rep. 13, 73–77.
Fu, X.-L., Hou, F., Liu, F.-R., Ren, S.-W., Cao, J.-T., Liu, Y.-M., 2019. Biosens. Bioelectron. 129, 72–78.
Gai, Q.-Q., Wang, D.-M., Huang, R.-F., Liang, X.-X., Wu, H.-L., Tao, X.-Y., 2018. Biosens. Bioelectron. 118, 80–87.
Granato, T., Porpora, M.G., Longo, F., Angeloni, A., Manganaro, L., Anastasi, E., 2015. Clin. Chim. Acta 446, 147–155.
Hu, L., Zheng, J., Zhao, K., Deng, A., Li, J., 2018. Biosens. Bioelectron. 101, 260–267.
Hu, G.-B., Xiong, C.-Y., Liang, W.-B., Yang, Y., Yao, L.-Y., Huang, W., Luo, W., Yuan, R., Xiao, D.-R., 2019. Biosens. Bioelectron. 135, 95–101.
Li, Y., Zhang, N., Zhao, W.-W., Jiang, D.-C., Xu, J.-J., Chen, H.-Y., 2017. Anal. Chem. 89, 4945–4950.
Li, S., Liu, Z., Li, J., Chen, A., Chai, Y., Yuan, R., Ying, Z., 2018. ACS Appl. Mater. Interfaces 10, 14483–14490.
Lichan, C., Yuwu, C., Xiaoxue, Z., Yuanjin, Z., Guonan, C., 2009. Anal. Chem. 81, 2394–2398.
Lin, Z., Wang, W., Jiang, Y., Qiu, B., Chen, G., 2010. Electrochim. Acta 56, 644–648.
Lin, Y., Shen, R., Liu, N., Yi, H., Dai, H., Lin, J., 2018. Anal. Chim. Acta 1035, 175–183.
Lu, K.H., 2018. Jama 319, 557–558.
Melchior, S.A., Palaniyandy, N., Sigalas, I., Iyuke, S.E., Ozoemena, K.I., 2019. Electrochim. Acta 297, 961–973.
Sha, H., Zhang, Y., Wang, Y., Ke, H., Xiong, X., Jia, N., 2019. Biosens. Bioelectron. 124–125, 59–65.
Sheydaei, M., Shiadeh, H.R.K., Ayoubi-Feiz, B., Ezzati, R., 2018. Chem. Eng. J. 353, 138–146.
Shi, X.-M., Mei, L.-P., Wang, Q., Zhao, W.-W., Xu, J.-J., Chen, H.-Y., 2018. Anal. Chem. 90, 4277–4281.
Sun, F., Wang, Z., Feng, Y., Cheng, Y., Ju, H., Quan, Y., 2017. Biosens. Bioelectron. 100, 28–34.
Tajmul, M., Parween, F., Singh, L., Mathur, S.R., Sharma, J.B., Kumar, S., Sharma, D.N., Yadav, S., 2018. Int. J. Biol. Macromol. 108, 503–514.
Tan, Y., Li, M., Ye, X., Wang, Z., Wang, Y., Li, C., 2018. Sens. Actuators B Chem. 262, 982–990.
Wang, M., Hu, M., Hu, B., Guo, C., Song, Y., Jia, Q., He, L., Zhang, Z., Fang, S., 2019. Biosens. Bioelectron. 135, 22–29.
Zhang, H., Zhuo, Z., Chen, L., Chen, C., Luo, F., Chen, Y., Guo, L., Qiu, B., Lin, Z., Chen, G., 2018. Electrochem. Commun. 88, 75–78.
Zhang, H., Luo, F., Wang, P., Guo, L., Qiu, B., Lin, Z., 2019. Biosens. Bioelectron. 129, 36–41.
Zuo, F., Han, Z., Ji, X., Chen, S., Yuan, R., 2018. Electrochim. Acta 271, 173–179.
Zuo, F., Zhang, H., Xie, J., Chen, S., Yuan, R., 2018. Electrochim. Acta 271, 173–179.